Electromechanical transition in quantum dots

G. Micchi, R. Avriller, and F. Pistolesi

University of Bordeaux, LOMA, UMR 5798, Talence, France
and CNRS, LOMA, UMR 5798, F-33400 Talence, France
(Received 28 July 2016; published 13 September 2016)

The strong coupling between electronic transport in a single-level quantum dot and a capacitively coupled nanomechanical oscillator may lead to a transition towards a mechanically bistable and blocked-current state. Its observation is at reach in carbon-nanotube state-of-art experiments. In a recent publication [Phys. Rev. Lett. **115**, 206802 (2015)] we have shown that this transition is characterized by pronounced signatures on the oscillator mechanical properties: the susceptibility, the displacement fluctuation spectrum, and the ring-down time. These properties are extracted from transport measurements, however the relation between the mechanical quantities and the electronic signal is not always straightforward. Moreover the dependence of the same quantities on temperature, bias or gate voltage, and external dissipation has not been studied. The purpose of this paper is to fill this gap and provide a detailed description of the transition. Specifically we find (i) the relation between the current-noise and the displacement spectrum; (ii) the peculiar behavior of the gate-voltage dependence of these spectra at the transition; (iii) the robustness of the transition towards the effect of external fluctuations and dissipation.

I. INTRODUCTION

Detection and actuation of mechanical systems at the nanoscale is a present-day challenge that has important fundamental and application perspectives [1–8]. Electronic transport allows for detection of the displacement of extremely small mechanical oscillators, like carbon nanotubes [9]. Increasing the coupling between electronic transport and mechanical displacement allows for a more sensitive detection and more precise actuation of the mechanical motion. However, strong coupling can also lead to an unexpected behavior of the system, as it was recognized in studying coherent electronic transport in molecular junctions coupled to low-frequency (classical) vibrations [10,11]. In nanomechanical systems the importance of the electron back-action on the mechanical degrees of freedom was recognized very early [12–17], and concerned the case of oscillators coupled to single-electron transistors in the orthodox incoherent Coulomb blockade regime. In this regime it was found that for sufficiently strong coupling the system presents a mechanical bistability with a suppression of the current [18], analogous to the coherent case of molecular junctions [19]. In both cases the transition to the bistable state is controlled by the intensity of the electromechanical coupling ϵ_P, defined as F_0^2/k, where k is the spring constant of the oscillator and F_0 is the force acting on the oscillator when one electron is added to the quantum dot or to the metallic island of the single-electron transistor. The bistability and suppression of the current is expected when both the temperature T and the bias voltage V are smaller than ϵ_P (we work throughout the paper with the notation that the electric charge e, the Boltzmann constant k_B, and the reduced Planck constant $\hbar$ are equal to 1). In the coherent transport case an additional condition has to be satisfied: ϵ_P larger than Γ, the typical width of the electron state. Observation of this effect is not easy, since in general the value of ϵ_P is very small. In order to increase its value it has been proposed, for instance, to study a mechanical system close to the Euler-buckling instability, since there k vanishes, leading to an increase of two orders of

magnitude of ϵ_P [20–22]. However the transition has not been observed yet, contrary to the related, but different, effect known as the Franck-Condon blockade [23–26]. The latter concerns high-frequency phonons in the regime $\Gamma \ll T \ll \omega_0$, where $\omega_0/2\pi$ is the phonon frequency.

The experimental situation changed recently with the impressive progress that has been achieved in the detection and manipulation of carbon-nanotube mechanical oscillators. After the observation of the mechanical resonance [9] it has been possible to observe the back-action of single-electron transport on the mechanical mode [27,28]. This opened the way to an impressive series of applications for mass [3,29], force [7], magnetic [30] and biological sensors [31], high quality factor resonators [32,33], as well as the observation of phenomena related to the nonlinear behavior of the oscillator [34,35]. In particular, recently the group of S. Ilani reported the observation of devices with values of ϵ_P of the order of 0.3 K [36,37]. The system they study is well modelled by a quantum dot coupled to a mechanical oscillator. In a very recent publication we investigated some of the features expected when the transition is studied varying the coupling constant ϵ_P at low temperature ($\omega_0 \ll V,T \ll \epsilon_P$) [38]. Specifically we found that the mechanical mode softens at the transition to the bistable state, with a minimal value controlled by the bias voltage, and that phase fluctuations dominate the dynamics leading to a universal quality factor of 1.71. This provided a glance on the transition scenario, but several points deserve to be investigated in order to clarify the full picture.

In this paper we analyze the current-noise spectrum and, in particular, we investigate its relation to the displacement spectrum. The two spectra may be proportional to each other, since the current is modulated by the displacement, but in general more complex relations exist.

One of the clearest proofs of the back-action of single-electron transport on the mechanical degrees of freedom is the observation of a weak softening of the mode as a function of the gate voltage around the degenerate point. Since at the transition the mode softens spectacularly, we investigate how

this reflects on the gate-voltage dependence of the mechanical resonance.

In general the system is out of equilibrium and the bias voltage plays the role of the temperature. Both the bias voltage and the temperature influence the transition, mainly smearing it. We thus investigate the region where its observation is still possible.

Finally real systems are always coupled to other degrees of freedom that induce dissipation. We consider the effect of the presence of a finite dissipation. We find that it can either have no effect on the main physical quantities, or improve the visibility of the transition when the temperature of the environment is lower than the bias voltage.

The plan of the paper is the following. In Sec. II we introduce the microscopic model describing a single-level quantum dot coupled to a mechanical oscillator; we present then a Langevin and Fokker-Planck description of the system dynamics. In Sec. III we derive the average electric current through the device. In Sec. IV we obtain and study the current-fluctuation spectrum relating it to the displacement spectrum. In Sec. V we study the gate voltage dependence of the aforementioned spectra. In Sec. VI the effect of thermal and off-equilibrium fluctuations is discussed. In Sec. VII the influence of an external damping is considered on the oscillator quality factor. Finally Sec. VIII gives our conclusions and perspectives.

II. MODEL AND PREREQUISITES

A. Model

Following the literature on the subject [11,38] we describe the quantum dot by a spinless single electronic level coupled to a mechanical oscillator. The Hamiltonian reads

$$H = H_L + H_R + H_T + (\epsilon_0 - F_0 x)d^\dagger d + \frac{p^2}{2m} + \frac{kx^2}{2}, \quad (1)$$

where d and ϵ_0 are the destruction operator and the energy of the electronic level on the dot, respectively, x is the displacement of the relevant mechanical mode, p is its conjugated momentum, m is the mode effective mass, k is the spring constant (with $\omega_0 = \sqrt{k/m}$), and F_0 is the electrostatic force acting on the oscillator when the electronic level is occupied. The first three terms describe the leads and their coupling to the electronic level: $H_\alpha = \sum_k (\epsilon_{\alpha k} - \mu_\alpha)c_{\alpha k}^\dagger c_{\alpha k}$, $H_T = \sum_k t_\alpha c_{\alpha k}^\dagger d$ + H.c., with $\alpha = L(R)$ for the left (right) lead, c and $\epsilon_{\alpha k}$ the destruction operator and the energy of the electrons in the leads, respectively, and μ_α the chemical potential. From these quantities one can define the lead's tunneling rate $\Gamma_\alpha \equiv \pi t_\alpha^2 \rho_\alpha$ with ρ_α the density of states and the single-level width $\Gamma \equiv \Gamma_L + \Gamma_R$. For simplicity in the following we choose $\Gamma_L = \Gamma_R = \Gamma/2$ and $\mu_L = -\mu_R = V/2$, with V the bias voltage. In the following we will always consider the regime that is realized in current experiments with carbon nanotubes. This corresponds to the limit $\Gamma_\alpha \gg \omega_0$ and $\omega_0 \ll \max(T,V)$ that allows one to solve the problem within the Born-Oppenheimer approximation and to treat the mechanical mode classically [11]. We will not consider in this paper the case of strongly coupled fast (quantum) oscillator, that is more relevant for molecular transport [25,39–41].

B. Classical stochastic description

With these assumptions the displacement dynamics of the mechanical mode can be described by a Langevin equation:

$$m\ddot{x} + A(x)\dot{x} + m\omega_0^2 x = F_e(x) + \xi(t), \quad (2)$$

where the charge fluctuations on the dot are at the origin of the average force $F_e(x)$, the dissipation $A(x)$, and the stochastic force $\xi(t)$, that satisfies $\langle \xi(t)\xi(t')\rangle = D(x)\delta(t - t')$ (actually the time range of the correlation function is Γ^{-1}, but since $\Gamma \gg \omega_0$ we approximate it by a Dirac δ function) [11,18]. The coefficients read $F_e(x) = F_0 n(x)$, $D(x) = F_0^2 S_{nn}(x,\omega = 0)$, $A(x) = -F_0^2(\partial S_{nn}/\partial \omega)(x,\omega)|_{\omega=0}$, with $n = d^\dagger d$, $n(x) = \langle n \rangle$ the average occupation of the dot, and $S_{nn}(x,\omega) = \langle n(t)n(0)\rangle_\omega$ the charge fluctuation spectrum. The explicit expression for A, F_e, and D has been obtained in Ref. [11] (we provide an alternative and more elementary derivation in Appendix):

$$\langle n \rangle = \int_{-\infty}^{+\infty} \frac{d\omega}{2\pi\Gamma}(f_L + f_R)\tau, \quad (3)$$

$$S_{nn}|_{\omega=0} = \sum_{\alpha,\beta} \int_{-\infty}^{+\infty} \frac{d\omega}{2\pi\Gamma^2} f_\alpha(1 - f_\beta)\tau^2, \quad (4)$$

$$\frac{dS_{nn}}{d\omega}\bigg|_{\omega=0} = \sum_{\alpha,\beta} \int_{-\infty}^{+\infty} \frac{d\omega}{2\pi\Gamma^2} f_\alpha\tau[f_\beta'\tau - (1 - f_\beta)\tau'], \quad (5)$$

where $f_\alpha(T,\omega) = f_F(\omega - \mu_\alpha)$, $f_F(\omega) = (1 + e^{\omega/T})^{-1}$ is the Fermi function, $\tau(\omega,x) = 1/\{1 + [(\omega - \epsilon_0 + F_0 x)/\Gamma]^2\}$ is the energy-dependent electronic transmission factor through the quantum dot, and the prime in Eq. (5) indicates the derivative with respect to ω.

Since the stochastic force is short-ranged in time one can derive a Fokker-Planck equation for the probability distribution $P(x,p,t)$ [13,42]:

$$\partial_t P = \frac{p}{m}\partial_x P - F\partial_p P + \frac{A}{m}\partial_p(pP) + \frac{D}{2}\partial_p^2 P, \quad (6)$$

where $F(x) = -kx + F_e(x)$.

C. Effective potential determined by $F(x)$

The total deterministic force $F(x)$ acting on the oscillator is given by the sum of the mechanical restoring force $-kx$ and of the electronic contribution $F_0\langle n \rangle$. For vanishing temperature (the finite temperature case will be discussed in Sec. VI) and arbitrary bias voltage one finds

$$F(x) = -kx + \frac{F_0}{2} + \frac{F_0}{2\pi}\sum_{\alpha=\pm}\arctan\frac{\alpha V/2 - \epsilon_0 + F_0 x}{\Gamma}. \quad (7)$$

One can verify that for $\epsilon_0 = \epsilon_P/2$ the force is antisymmetric with respect to the point $x_0 = F_0/2k$. This value of the gating is special and corresponds to the new electron-hole symmetry point for the system. We will focus mainly on this case in the remainder of the paper, dedicating Sec. V to a discussion on the ϵ_0 dependence of different physical quantities. The force is more conveniently expressed in terms of the dimensionless variable $y = F_0(x - x_0)/\Gamma$, for which one can write a Taylor

expansion in y:

$$F(y) = F_0 \sum_{n=0}^{\infty} a_{2n+1} y^{2n+1}, \quad (8)$$

with

$$a_1 = -\Gamma/\varepsilon_P + \arctan'(V/2\Gamma)/\pi \quad (9)$$

and $a_n = \arctan^{(n)}(V/2\Gamma)/[\pi n!]$ for $n > 1$. From the form of F follows immediately the form of the effective potential defined as

$$U(x) = -\int^x F(x')dx'. \quad (10)$$

As a function of y it reads $U(y) = -\Gamma \sum_{n=0}^{\infty} a_{2n+1} y^{2n+2}/(2n+1)$. The condition $a_1 < 0$ determines the stability of the minimum in $y = 0$ and gives the equation $\varepsilon_P < \varepsilon_c(V)$ with

$$\varepsilon_c(V) = \pi \Gamma \left(1 + \frac{V^2}{4\Gamma^2} \right) \quad (11)$$

defining the critical line. By graphical solution of the equation $F(y) = 0$ one finds that there is always one solution at $y = 0$, and then there can be one or two additional pairs of solutions at $\pm y_1$ and $\pm y_2$. Since the function is regular, the stationary points correspond either to maxima or minima of the potential, that alternate. Moreover the system has always at least one stable solution, thus when the solution at $y = 0$ is unstable there can be only two stable solutions at $\pm y_1$ (three solutions). This proves that in the region of the phase diagram $\varepsilon_P > \varepsilon_c(V)$ the potential has two symmetric minima (see also Fig. 1). The situation is more complex when the origin is stable ($a_1 < 0$), but a_3 and a_5 are not both negative. In this case the origin can be either the only minimum or two additional side minima may appear. By direct calculation one finds that $a_3 > 0$ for $V > 2\Gamma/\sqrt{3}$. Thus along the critical line this point $[\varepsilon_c(2\Gamma/\sqrt{3}) = 4\pi/3\Gamma]$ marks the beginning of the multistability. The full
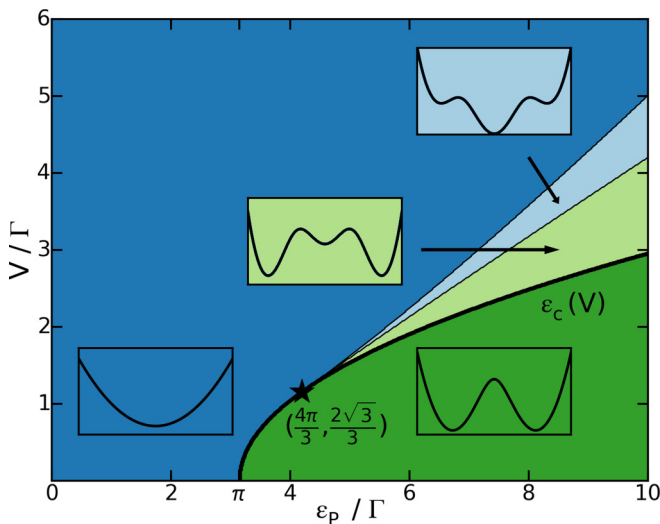
behavior is shown in Fig. 1, as obtained by numerically solving $F(y) = 0$.

In the following we will limit to voltages smaller than $2\Gamma/\sqrt{3}$, thus the two possible phases are the stable and bistable one, separated by the line $\varepsilon_c(V)$. For vanishing voltage and temperature the effective potential reads

$$U(y) = \frac{\Gamma}{2\varepsilon_P} y^2 - \frac{\Gamma}{2\pi} [2y \arctan y - \ln(1 + y^2)], \quad (12)$$

that expanded around $y = 0$ gives

$$U(y) = \frac{\Gamma}{2\pi} \frac{\pi \Gamma}{\varepsilon_P} \left[\left(1 - \frac{\varepsilon_P}{\pi \Gamma} \right) y^2 + \frac{1}{6} \frac{\varepsilon_P}{\pi \Gamma} y^4 + O(y^6) \right]. \quad (13)$$

In this case the transition takes place at the value $\varepsilon_P = \pi \Gamma = \varepsilon_c(0) \equiv \varepsilon_c$.

The first important consequence of the transition is the softening of the mechanical mode. Let us define

$$\omega_m^2 = -\frac{1}{m} \frac{dF}{dx} \quad (14)$$

for x at the minimum of the potential. This gives

$$\omega_m^2 = \omega_0^2 \left(1 - \frac{\varepsilon_P}{\varepsilon_c} \right) \quad (15)$$

for $\varepsilon_P \leqslant \varepsilon_c$ and

$$\omega_m^2 \approx 2\omega_0^2 \left(\frac{\varepsilon_P}{\varepsilon_c} - 1 \right) \quad (16)$$

for $\varepsilon_P \geqslant \varepsilon_c$ and $(\varepsilon_P - \varepsilon_c)/\varepsilon_c \ll 1$. As discussed in Ref. [38] the softening of the mechanical mode has important consequences that can be observed in the response functions.

The appearance of the bistability marks also the beginning of the reduction of the current, as we will discuss more in detail in the following. In Fig. 2 we provide a simple picture of the blockade: The presence of an electron changes also the stable position of the oscillator and consequently the energy of its level (ϵ_0). When the shift in the energy (ε_P) exceeds the bias voltage both the occupied and empty state are out of the

FIG. 1. Phase diagram for the stability of the effective potential in the V-ε_P plane for $\varepsilon_0 = \varepsilon_P/2$ and vanishing temperature. The thick line indicates the critical line ε_c.
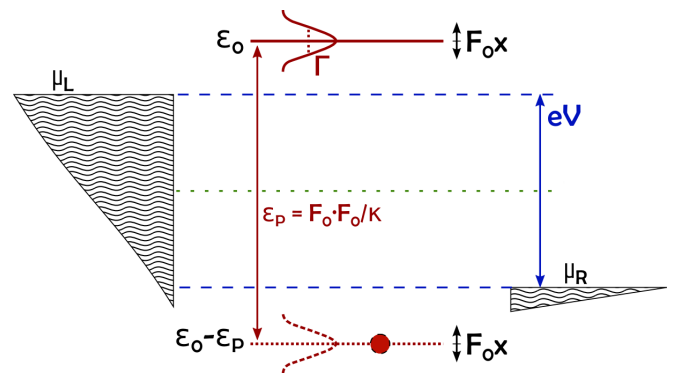

FIG. 2. A pictorial view of the current blockade mechanism. We show the position of the electronic level of the dot for the two stable positions of the oscillators depending on the state of the dot, empty (upper level) or full (lower level). When $\varepsilon_P > V$ both levels are out of the conducting window and for thus $\Gamma \ll V, \varepsilon_P$ the current cannot flow stabilizing both states. For Γ of the order of V and ε_P the picture is blurred by the finite width of the energy level, leading simply to a reduction of the current.

bias window, thus in a blocked current state. This holds strictly when $\Gamma \ll \varepsilon_P$, but in general a residual current is possible, due to the finite width in energy of the single electronic level.

D. Stationary solution for $V, T \ll \Gamma$

In the regime $V, T \ll \Gamma$ the stationary solution of the Fokker-Planck equation (6) can be found analytically. As a matter of fact the coefficients A and D depend weakly on x. In general when their ratio is independent of the position it is possible to define an effective temperature:

$$T_{\text{eff}} = \frac{D(x)}{2A(x)}. \tag{17}$$

One can verify by substitution that the function

$$P_{\text{st}}(x, p) = \mathcal{N}^{-1} e^{-E(x,p)/T_{\text{eff}}}, \tag{18}$$

solves Eq. (6). Here $E(x, p) = p^2/2m + U(x)$ is the oscillator energy, U is defined by Eq. (10), and $\mathcal{N} = \int dx \, dp \, \exp(-\frac{E(x,p)}{T_{\text{eff}}})$ is a normalization factor. The explicit expressions for A and D in the limit $V, T \ll \Gamma$ can be calculated by exploiting the weak ω dependence of $\tau(\omega, x)$ with respect to the fast variation of the Fermi functions. Expanding the expression of $\tau(\omega, x)$ around $\omega = 0$ and integrating in ω we obtain

$$A(x) = \frac{F_0^2}{\pi \Gamma^2} \tau_0^2(x) \left[1 + \frac{2\pi^2}{3} \left[5\tau_0(x) - 6\tau_0^2(x) \right] \left(\frac{T}{\Gamma} \right)^2 \right], \tag{19}$$

where $\tau_0(x) = \tau(0, x)$, with the remarkable relation

$$\frac{D(x)}{2A(x)} = \frac{T}{2} \left(1 + \frac{V}{2T} \coth \frac{V}{2T} + \cdots \right) \equiv T_{\text{eff}}. \tag{20}$$

We thus find that at lowest order in T/Γ and V/Γ the ratio D/A does not depend on x. This is not surprising for $V \ll T$, since in this case the system is essentially in equilibrium and $T_{\text{eff}} \approx T$, but it is somewhat unexpected for $(\Gamma \gg) V \gg T$, i.e., far from equilibrium. In this limit we find $T_{\text{eff}} \approx V/4$ that agrees with what is found for a metallic single-electron transistor in Ref. [12]. Most numerical simulations presented in this paper are performed for $V/\Gamma = 5 \times 10^{-3}$, thus in this regime.

From the form of the stationary solution it is clear that the effective potential plays a crucial role. It is thus convenient to introduce a parametrization of the phase space (x-p) of the oscillator in terms of the energy $E(x, p)$ and of the time along a trajectory of given energy:

$$t_E(x, p) = \frac{1}{(2m)^{1/2}} \int^x \frac{dx'}{[E(x', p) - U(x')]^{1/2}}. \tag{21}$$

The Jacobian of the transformation is unitary. In terms of the new variables the distribution is uniform along the trajectory, thus leading to the following form for the stationary distribution integrated over the trajectories:

$$P_{\text{st}}(E) = \frac{2\pi}{\omega(E)} e^{-E/T_{\text{eff}}} / \mathcal{N} \tag{22}$$

with $\mathcal{N} = \int dE \, 2\pi e^{-E/T_{\text{eff}}} / \omega(E)$, and $2\pi/\omega(E)$ the period of the trajectory of energy E.

Let us finally briefly discuss $\omega(E)$. This can be obtained analytically for the potential containing only the quadratic and quartic part [43,44]. We give its expression in the stable phase $\varepsilon_P < \varepsilon_c$:

$$\frac{\omega(E)}{\omega_0} = \frac{\pi}{2} \frac{\sqrt{B(E)}}{K[-m(E)]}, \tag{23}$$

with

$$B(E) = \frac{\varepsilon_c - \varepsilon_P}{2\varepsilon_c} + \sqrt{\frac{3(\varepsilon_c - \varepsilon_P)^2 \varepsilon_c + 4\pi^2 \varepsilon_P^2 E}{12\varepsilon_c^3}},$$

$$m(E) = \frac{\sqrt{(\varepsilon_c - \varepsilon_P)^2 + 4\pi^2 \varepsilon_P^2 E/3\varepsilon_c} - (\varepsilon_c - \varepsilon_P)}{\sqrt{(\varepsilon_c - \varepsilon_P)^2 + 4\pi^2 \varepsilon_P^2 E/3\varepsilon_c} + (\varepsilon_c - \varepsilon_P)}$$

and $K[-m(E)]$ the complete elliptic integral of the first kind with parameter $-m(E)$. At the critical point $\varepsilon_P = \varepsilon_c$ the expression simplifies:

$$\frac{\omega(E)}{\omega_0} = \left(\frac{\pi^3}{48} \right)^{1/4} \frac{\Gamma[3/4]}{\Gamma[5/4]} (E/\Gamma)^{1/4} \approx 1.212(E/\Gamma)^{1/4}, \tag{24}$$

with $\Gamma[x]$, the Euler-Γ function. In the other limit, for $\varepsilon_P \ll \varepsilon_c$ one can expand in E obtaining

$$\omega(E) = \omega_m + \omega' E \tag{25}$$

with

$$\omega' \equiv \frac{d\omega_m}{dE} = \frac{\pi^2 \omega_0}{4\varepsilon_c} \left(\frac{\varepsilon_P}{\varepsilon_c} \right)^2 \left(1 - \frac{\varepsilon_P}{\varepsilon_c} \right)^{-3/2}. \tag{26}$$

In the next sections we will consider in some detail how different physical quantities behave as a function of the coupling strength ε_P, particularly at the transition to the bistable phase.

III. ELECTRONIC CURRENT

We begin by considering the current flowing through the quantum dot. In the classical regime considered in this paper for given value of x one can write

$$I(x) = \int \frac{d\omega}{2\pi} \tau(\omega, x)[f_L(\omega) - f_R(\omega)]. \tag{27}$$

The current is the average of this quantity over the positions visited by the oscillator:

$$I(t) = \int \frac{d\omega}{2\pi} \int dx \, dp \, P(x, p, t) I(x). \tag{28}$$

In the stationary regime I does not depend on t and one can use the stationary distribution for the probability. We define the low voltage conductance as $G(V) = I/V$ for small V. For $T = 0$ and $V \ll \Gamma$ it reads

$$G(V) = G_Q \int dx \, dp \, P_{\text{st}}(x, p) \tau(0, x) + O(V/\Gamma), \tag{29}$$

where $G_Q = 1/2\pi$ is the quantum of conductance in the units $\hbar = e = 1$. Figure 3 shows the conductance evaluated numerically from Eq. (29) for different values of V, $T = 0$, and $\varepsilon_0 = \varepsilon_P/2$. The extreme limit $V \to 0$ shows very well the presence of a transition for $\varepsilon_P = \varepsilon_c$, the conductance is flat for $\varepsilon_P < \varepsilon_c$ and decreases smoothly for $\varepsilon_P > \varepsilon_c$, with a cusp at
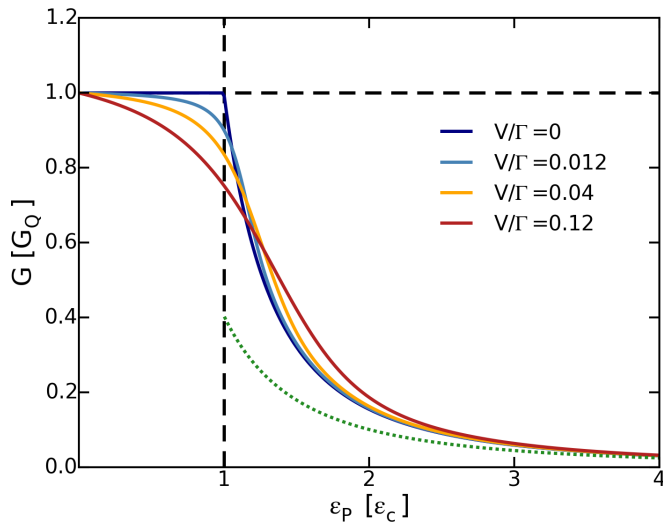
FIG. 3. Conductance as a function of the coupling constant ε_P for $T = 0$ and different values of V as indicated in the legend. The dotted (green) line is the asymptotic behavior of the conductance obtained for $\varepsilon_P \gg \varepsilon_c$, when the system is in the bistable phase.

$\varepsilon_P = \varepsilon_c$. Already at this value it is clear that the suppression of the current is relatively slow as a function of the coupling. This is due to the Lorentzian decay of the transparency τ as a function of the energy. For higher values of the voltage the transition is smooth.

When the effective potential is truncated to fourth order [cf. Eq. (13)] it is possible to obtain an analytic expression of the conductance. The dot transparency can be expressed as a power series of y: $\tau(0,x) = \sum_{n=0}^{+\infty} (-1)^n y^{2n}$. By expanding the y^4 term in the exponential of the stationary distribution one can evaluate all the Gaussian integrals for $\varepsilon_P \leqslant \varepsilon_c$ obtaining for the conductance

$$\langle G \rangle = G_Q \sum_{n=0}^{+\infty} (-1)^n \left(\frac{12\pi^2 T_{\text{eff}}}{\varepsilon_c} \right)^{n/2} \Xi_n[\alpha] \qquad (30)$$

with

$$\Xi_n[\alpha] = \frac{\sum_{p=0}^{+\infty} \frac{(-\alpha)^p}{p!} \mathbf{\Gamma}\left[\frac{1+2(n+p)}{4} \right]}{\sum_{p=0}^{+\infty} \frac{(-\alpha)^p}{p!} \mathbf{\Gamma}\left[\frac{1+2p}{4} \right]}, \qquad (31)$$

$\alpha = (\varepsilon_c - \varepsilon_P)/\varepsilon_P \sqrt{3\varepsilon_c/\pi^2 T_{\text{eff}}} \geqslant 0$.

The expression simplifies for $\varepsilon_P \ll \varepsilon_c$:

$$G = G_Q \left(1 - \frac{\pi^2}{4} \frac{\varepsilon_P V}{\varepsilon_c^2} \right). \qquad (32)$$

Close to the transition (specifically for $\alpha \ll 1$) we find

$$G(V) \approx G_Q \left\{ 1 - \left(\frac{3\pi^2 V}{\varepsilon_c} \right)^{1/2} \frac{\mathbf{\Gamma}[3/4]}{\mathbf{\Gamma}[1/4]} \right.$$
$$\left. - 6 \frac{\varepsilon_c - \varepsilon_P}{\varepsilon_P} \frac{\mathbf{\Gamma}[3/4]}{\mathbf{\Gamma}[1/4]} \left[\frac{\mathbf{\Gamma}[3/4]}{\mathbf{\Gamma}[1/4]} - \frac{\mathbf{\Gamma}[5/4]}{\mathbf{\Gamma}[3/4]} \right] \right\}. \qquad (33)$$

This indicates that $G(V)$ decreases rapidly with V at criticality, as can be seen in the figure.

Finally we investigate the behavior deep in the bistable regime. For $\varepsilon_P \gg \varepsilon_c$ the two stable solutions are at $y = \pm \varepsilon_P / 2\Gamma$. By simply taking the value of the transparency for these values of y we have

$$G = \frac{G_Q}{1 + (\pi \varepsilon_P / 2\varepsilon_c)^2}. \qquad (34)$$

The conductance vanishes as a power law for large coupling. We show this curve dotted in Fig. 3. This value can be corrected by taking into account the Gaussian fluctuations around the two minima that add a correction $1 + 3\varepsilon_c V / 2\varepsilon_P^2$ that increases the conductance a bit by increasing the effective temperature.

In conclusion we have seen that the current is slowly suppressed as a function of the coupling constant, but in general there is not a spectacular effect at the transition. This is in contrast to what happens for large values of the coupling and finite voltage $V \gg \Gamma$, for which the current has quite a sharp dependence on the voltage [19]. In the following we will consider the current-noise spectrum. We will see that it is directly related to the mechanical dynamics and presents thus clear signatures of the transition.

IV. POWER SPECTRAL DENSITY OF CURRENT FLUCTUATIONS

The interest in the measurement of the current-fluctuation spectrum is that it allows one to detect the motion of the mechanical oscillator without driving it. The current is modulated by a variation of the displacement, thus each fluctuation of the displacement will appear also as a fluctuation of the current. In Ref. [38] we have investigated in some details the behavior of the displacement fluctuation spectrum $[S_{xx}(\omega)]$ at the transition. As it can be seen from Eqs. (15) and (16) the mechanical mode becomes soft at the transition as predicted by the effective potential behavior. At the transition the fluctuations are very strong, and the meaning of mechanical mode is not so clear anymore. That is why it is necessary to consider measurable manifestations of the mechanical dynamics. The study of the displacement fluctuation spectrum allows us to follow the evolution of the mechanical mode and to see its behavior at the transition. We refer to Ref. [38] for a detailed discussion, but it may be useful to recall the main features: The position of the main peak of the spectrum has a minimum as a function of the coupling constant at $\varepsilon_P = \varepsilon_c$; the minimum value is not zero, but a finite value that is controlled by the bias voltage (or the effective temperature). It vanishes like $(T_{\text{eff}} / \Gamma)^{1/4}$ and the quality factor is universal with value 1.7. The displacement spectrum is related to the response function to an external weak driving force by a relation of the fluctuation-dissipation kind. A direct measurement can be possible by detection of the current noise. But the relation between the displacement fluctuation spectrum and the current fluctuation spectrum is not always straightforward, in particular close to the transition. In this section, we discuss the behavior of the current-correlation function and its relation to the displacement fluctuation spectrum.

We begin with its definition:

$$S_{II}(\omega) = \frac{1}{2} \int_{-\infty}^{+\infty} dt\, e^{i\omega t} \langle \tilde{I}(t)\tilde{I}(0) + \tilde{I}(0)\tilde{I}(t) \rangle, \qquad (35)$$

where $\tilde{I}(t) = I(t) - \langle I \rangle$ is the quantum current operator (note that we define the spectrum with a factor of 1/2 with respect to the usual convention for quantum noise). The time-scale separation between the fast electronic degrees of freedom and the slow mechanical ones allows us to distinguish the purely electronic contribution to the current noise, coming from the granularity of the charge, and the one coming from the slow fluctuations of the position of the oscillator.

Let us first discuss briefly the electronic contribution. For fixed and given x the electronic noise reads $S_{II}^e(\omega \ll \Gamma) = \tau(x)[1 - \tau(x)]\langle I \rangle$ [45]. The spectrum is flat for $\omega \ll \Gamma$, and to obtain the observed value it is sufficient to average the above expression with $P(x, p)$. In the following we will neglect this contribution, since it has no frequency dependence at the interesting mechanical frequencies.

We thus consider only the current fluctuations originating from the displacement fluctuation. We can then write

$$S_{II}(\omega) = \int_{-\infty}^{+\infty} dt \, e^{i\omega t} \langle \tilde{I}[x(t)] \tilde{I}[x(0)] \rangle, \quad (36)$$

with $I(x)$ given by Eq. (27). Starting from this expression one can compute numerically the average current following the method presented in Ref. [19]. It implies the numerical solution of the Laplace transform of the Fokker-Planck equation and it gives

$$S_{II}(\omega) = -2\text{Tr}\left[(\hat{I} - \langle I \rangle)\frac{\mathcal{L}_0}{\omega^2 + \mathcal{L}_0^2}(\hat{I} - \langle I \rangle)P_{\text{st}}\right], \quad (37)$$

where $\hat{I}$ is the operator that at each point in the x-p phase space associates the current Eq. (27), $\mathcal{L}_0$ is the Fokker-Planck matrix that comes from writing Eq. (6) as $\partial_t P = \mathcal{L}_0 P$, and P_{st} is the steady-state solution satisfying $\mathcal{L}_0 P_{\text{st}} = 0$.

We will use this numerical method in the following, but first it is instructive to study the explicit relation between the current spectral density and the displacement spectrum defined as

$$S_{xx}(\omega) = \int_{-\infty}^{+\infty} e^{i\omega t} \langle \tilde{x}(t)\tilde{x}(0) \rangle dt, \quad (38)$$

with $\tilde{x}(t) = x(t) - \langle x \rangle$. Since we are mainly concerned with the case $V, T \ll \Gamma$ we can linearize the current in the voltage. The current correlation function can then be written as

$$S_{II}(t) = G_Q^2 V^2 \langle \tilde{\tau}[x(t)] \tilde{\tau}[x(0)] \rangle, \quad (39)$$

where $\tilde{\tau} = \tau - \langle \tau \rangle$. This expression shows that the relation between S_{II} and S_{xx} depends on the regime considered. When the relevant dependence of τ on x is linear the result may be a direct proportionality, but in general a more complex relation exists.

Finally the current correlator can be calculated analytically in the regime of very small damping rate $A/m \ll \Delta\omega$, with $\Delta\omega$ the width of the main peak in the spectral density induced by the oscillator nonlinearity [38]. Following the method introduced by Dykman *et al.* [44] and Ref. [38], the autocorrelation function for the current fluctuations in this regime can be well approximated by

$$\frac{S_{II}(t)}{(G_Q V)^2} = \int_0^{+\infty} dE \int_0^{2\pi/\omega(E)} d\tau \, P_{\text{st}}(E, \tau) \tilde{\tau}$$
$$\times [x_E(t+\tau)] \tilde{\tau}[x_E(\tau)], \quad (40)$$

where $x_E(t)$ is the function with period $2\pi/\omega(E)$ that satisfies the equation of motion $m\ddot{x} = F(x)$ for given energy $E = p^2/2m + U(x)$. In the next subsections we present the results for the current spectrum in different regimes.

A. S_{II} in the monostable phase $\varepsilon_P \leqslant \varepsilon_c$

For $\varepsilon_P \leqslant \varepsilon_c$ (and $V, T \ll \Gamma$) the effective potential has a single minimum at $x = F_0/2k$, around which the system oscillates. When the amplitude of these oscillations is sufficiently small (essentially for $T_{\text{eff}} \ll \Gamma$, see also the section on the finite temperature) we can expand the transmission factor to second order in x:

$$\tau[x(t)] \approx 1 - [F_0 x(t)/\Gamma]^2. \quad (41)$$

This leads to the following expression for the current fluctuations:

$$S_{II}(t) \approx (G_Q V)^2 \left(\frac{F_0}{\Gamma}\right)^4 \langle \tilde{x}^2(t)\tilde{x}^2(0) \rangle. \quad (42)$$

This relation allows one to relate the current spectrum to the displacement spectrum only in the weak-coupling regime where the position fluctuations are still Gaussian. In this case using Wick theorem we obtain

$$S_{II}(t) \approx 2(G_Q V)^2 \left(\frac{F_0}{\Gamma}\right)^4 S_{xx}^2(t), \quad (43)$$

or equivalently its Fourier transform,

$$S_{II}(\omega) = 2(G_Q V)^2 \left(\frac{F_0}{\Gamma}\right)^4 \int_{-\infty}^{+\infty} \frac{d\omega'}{2\pi} S_{xx}(\omega - \omega') S_{xx}(\omega'). \quad (44)$$

For extremely small $\varepsilon_P \ll \varepsilon_c$ the displacement spectrum $S_{xx}(\omega)$ shows two Lorentzian peaks at frequencies $\pm\omega_m$ whose width is dominated by the dissipation $A/m \gg \Delta\omega$. In this regime $S_{II}(\omega)$ will thus show three Lorentzian peaks, centered at $\omega = 0$ and $\omega = \pm 2\omega_m$ with a width of $2A/m$. As discussed in Ref. [38] the nonlinear terms in the potential generate a finite width in the displacement spectrum $\Delta\omega$, and when $\Delta\omega \gg A/m$ [for $\varepsilon_P \ll \varepsilon_c$ the condition reads $(V/\omega_0)(\varepsilon_P/\varepsilon_c) \gg 1$] the Gaussian approximation cannot be used anymore to evaluate S_{II}. We can nevertheless directly calculate the current spectrum using Eq. (40). We restrict to the (dominant) first harmonics ($n = \pm 1$) in the Fourier series $x_E(t) = \sum_{n=-\infty}^{+\infty} e^{-in\omega(E)t} x_n(E)$. Expanding $\omega(E)$ in E one finds that the spectral density has two contributions:

$$S_{II}(\omega) \approx S_{II}^{\text{reg}}(\omega) + S_{II}^{\text{sing}}(\omega), \quad (45)$$

a regular [$S_{II}^{\text{reg}}(\omega)$] and a singular [$S_{II}^{\text{sing}}(\omega)$] one. They read

$$\frac{S_{II}^{\text{reg}}(\omega)}{(G_Q V)^2} = \frac{\pi}{4}\left(\frac{\varepsilon_P}{\Gamma}\right)^2 \frac{\omega_m T_{\text{eff}}}{|\omega'|\Gamma^2\omega} f_1\left(\frac{\omega - 2\omega_m}{2\omega' T_{\text{eff}}}\right), \quad (46)$$

$$\frac{S_{II}^{\text{sing}}(\omega)}{(G_Q V)^2} = \frac{7\pi^5}{2} \frac{\varepsilon_P^2}{\varepsilon_c^4} \frac{\omega_0^4}{\omega_m^4} T_{\text{eff}}^2 \delta(\omega) \quad (47)$$

with $f_1(u) = u^2 e^{-u}$. The singular contribution in reality is broadened by the dissipative term that if included in the calculation would give a width $2A/m$. Note that this sharp low-frequency contribution is not related to telegraph noise, as is the case in the bistable phase, since there is a single
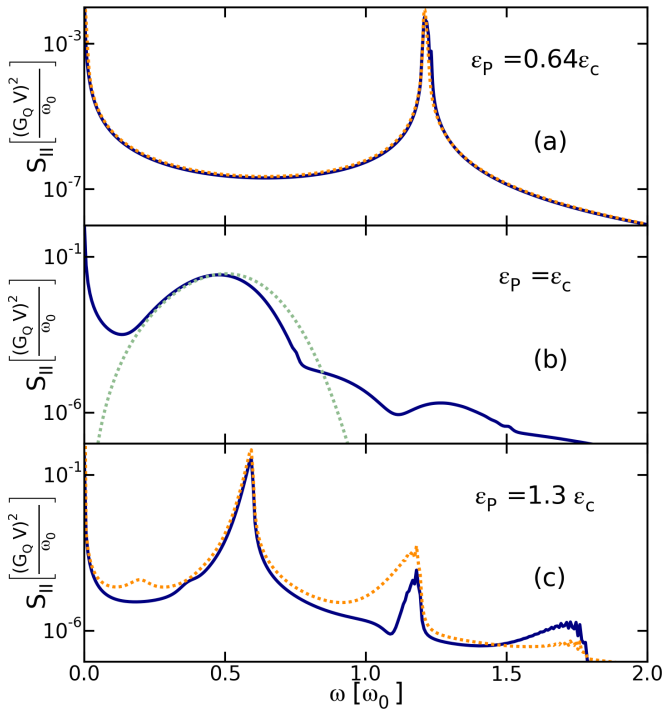
FIG. 4. Power spectral density of current fluctuations $S_{II}(\omega)$ for different values of the coupling constant $\varepsilon_P/\varepsilon_c = 0.64, 1, 1.3$ (as indicated in each panel) and for $\Gamma/\omega_0 = 10^3$, $V/\Gamma = 5 \times 10^{-3}$, $T = 0$. Blue solid lines give the result of the numerical evaluation of Eq. (37), while dotted lines show analytical results: In panel (a) the (orange) dotted line represents the convolution of the mechanical fluctuations $S_{xx}(\omega)$, as given in Eq. (44). In panel (b) the (green) dotted line gives the analytical result of current fluctuations coming from Eq. (49). In panel (c) the (orange) dotted line is proportional to S_{xx}, as written in Eq. (53).

minimum of the potential. The location ω_M of the maximum of the power spectral density and the full width at half maximum $\Delta\omega$ of the spectral line read

$$\omega_M = 2(\omega_m + 2\omega' T_{\text{eff}}) \tag{48}$$

with a width $\Delta\omega \approx 6.79\omega' T_{\text{eff}}$. We also notice that the width is roughly twice the width found for the displacement spectrum and the position of the maximum is exactly at twice the position of the maximum of the displacement spectrum. The numerical results obtained from Eq. (37) in this regime are shown in Fig. 4(a). A comparison with the analytical calculation (dotted line) shows that the agreement is very good. We observe that the peak at vanishing frequency appears also in the non-Gaussian limit and that its width is of the same order of the width dominated by the nonlinear fluctuations of the peak at $\omega \approx 2\omega_m$.

We cannot extend the expansion too close to the critical point $\varepsilon_P = \varepsilon_c$, but exactly at the critical point the potential is purely quartic, $U(y) = (\Gamma/12\pi)y^4$, and thus we can evaluate Eq. (40) analytically. The first harmonics of the oscillator displacement reads $x_1(E) = \alpha_1\Gamma/F_0(12\pi E/\Gamma)^{1/4}$ with a numerical factor $\alpha_1 \approx -0.477$ (see Supplemental Material of Ref. [38]). The spectrum has the form given by

Eq. (45) with

$$S_{II}^{\text{reg}}(\omega) \approx B_1 \frac{(G_Q V)^2}{\omega_0}\left(\frac{T_{\text{eff}}}{\Gamma}\right)^{3/4} f_2\left(\frac{\omega}{\omega_M}\right), \tag{49}$$

$$S_{II}^{\text{sing}}(\omega) \approx B_2(G_Q V)^2 \frac{T_{\text{eff}}}{\Gamma}\delta(\omega), \tag{50}$$

with a universal line shape of the resonance given by $f_2(u) = u^6 e^{-3/2(u^4-1)}$ and $B_1 = \alpha_1^4 96\Gamma[5/4]\pi^{5/4}3^{7/4}(2e)^{-3/2}/\Gamma[3/4]^2 \approx 6.797$, $B_2 = \alpha_1^4 24\pi^2[4\Gamma[7/4] - \Gamma[5/4]^2/\Gamma[3/4]]/\Gamma[3/4] \approx 30.2$.

From these expressions we infer that the maximum position and its width are

$$\omega_M \approx B_3\,\omega_0\left(\frac{T_{\text{eff}}}{\Gamma}\right)^{1/4}, \quad \Delta\omega \approx 0.479\,\omega_M, \tag{51}$$

with $B_3 = \pi^{3/4}\Gamma[3/4]2^{-1/4}/\Gamma[5/4] \approx 2.68$. In analogy to what found in Ref. [38] for the width of the displacement spectrum, we find that the peak in the noise spectrum has a universal quality factor of $Q = (\omega_M/\Delta\omega) \approx 2.09$. We note however that this differs from the one obtained for the displacement spectrum that is 1.71. The difference is a signature of the non-Gaussian fluctuations, that breaks the simple relation (44). In Fig. 4(b) we compare the prediction of Eq. (49) (green-dotted line) with the full numerical calculation obtained with Eq. (37) (full line). The overall shape of the main peak is well reproduced. We verified that the small overestimation (the plot is in logarithmic scale) of the peak width is due to the absence in the analytical calculation of the sixth-order term of the potential.

B. S_{II} in the bistable phase $\varepsilon_P > \varepsilon_c$

An analytical description is difficult close to the transition, but as soon as the potential minima become sufficiently deep, we can again describe the oscillator as a harmonic oscillator around the new minima. For $(\varepsilon_P \gg \varepsilon_c)$ thus the probability distribution becomes Gaussian around each minimum, related to the blocked current state in the occupied and empty electronic state. As a consequence, Wick theorem still holds if we expand displacement fluctuations separately around each minimum $y = \pm\pi\varepsilon_P/2\varepsilon_c$. We can thus evaluate Eq. (39) obtaining

$$S_{II}(t) = 2(G_Q V)^2\tau\left[(1-\tau)\frac{F_0^2 S_{xx}(t)}{\Gamma^2}\right.$$
$$+ \tau^3(3-4\tau)^2\left(\frac{F_0^2 S_{xx}(t)}{\Gamma^2}\right)^2$$
$$\left. + 12\tau(1-\tau)(1-2\tau)\frac{F_0^2\langle x^2\rangle}{\Gamma^2}\frac{F_0^2 S_{xx}(t)}{\Gamma^2}\right]. \tag{52}$$

[Note that we recover Eq. (43) for the weak-coupling regime if we set $\tau = 1$.] In the strong-coupling regime, $\tau \approx (2\varepsilon_c/\pi\varepsilon_P)^2 \ll 1$ and the dominating term in Eq. (52) is

$$S_{II}(\omega) \approx 2\left(G_Q V \frac{F_0}{\Gamma}\right)^2\tau(1-\tau)S_{xx}(\omega). \tag{53}$$

Deep in the bistable regime we thus find that a simple linear relation between $S_{II}(\omega)$ and $S_{xx}(\omega)$ holds. In Fig. 4(c) we plot

$S_{II}(\omega)$ obtained from Eq. (53) in orange-dotted line, compared to the full numerical calculation of Eq. (37). We see that all the features are well reproduced with a reasonably good quantitative agreement.

V. GATE VOLTAGE DEPENDENCE

One of the most spectacular and direct proofs of the back-action of the electronic transport on the mechanical dynamics is the observation of a maximum in the softening of the mechanical mode as a function of the gate voltage in coincidence with the maximum of the conductance of the quantum dot [27,28,37]. As we have seen, the softening of the mechanical mode is also a signature of the transition to the bistable phase, but so far we have discussed only its dependence on the coupling ε_P when the gate voltage is adjusted so that $\varepsilon_0 = \varepsilon_P/2$. In experiments the values of both ε_P and ε_0 are actually controlled by the value of the gate voltage. The first corresponds essentially to the number of excess electrons on the gate lead, while the second is linearly related to the gate voltage. Close to the symmetry point $\varepsilon_0 = \varepsilon_P/2$ one can neglect the weak gate voltage dependence of ε_P. It is then very interesting to study the behavior of the mechanical mode for small variation of the gate voltage close to the symmetry point for a given value of ε_P. As for the previous case it is understood that the mode cannot be characterized only by the value of its resonance, since the spectrum has typically a complex behavior. For this reason in this section we will study the displacement and current spectrum as a function of the gate voltage, or, as it appears in the present model, as a function of $\Delta\varepsilon_0 = \varepsilon_0 - \varepsilon_P/2$.

A. Softening of the mechanical mode from the effective potential

Let us begin from the behavior of ω_m as defined by Eq. (14). For $V = T = 0$ we can write the force as a function of y as follows:

$$\frac{F(y)}{F_0} = -\frac{\Gamma}{\varepsilon_P} y + \frac{1}{\pi} \arctan(y - \tilde{\varepsilon}_0), \qquad (54)$$

where $\tilde{\varepsilon}_0 = \Delta\varepsilon_0/\Gamma$. The presence of $\tilde{\varepsilon}_0$ changes the position of the solutions of $F(y) = 0$, but by graphical analysis one can verify that there can be only either one or three solutions. Applying the definition of ω_m by calculating the first derivative of $F(y)$ at y_0 one finds

$$\frac{\omega_m^2}{\omega_0^2} = 1 - \tau(y_0)\frac{\varepsilon_P}{\varepsilon_c}, \qquad (55)$$

where $\tau(y_0) = [1 + (y_0 - \tilde{\varepsilon}_0)^2]^{-1}$ is the transparency of the junction at the y_0 solution of the equation $F(y_0) = 0$. The equation for y_0 can be written as

$$y_0 = \frac{\varepsilon_P}{\varepsilon_c} \arctan(y_0 - \tilde{\varepsilon}_0). \qquad (56)$$

Equation (55) generalizes Eq. (15). It is exact, but finding the value of y_0 may require some approximations. We consider thus three limiting cases.

(i) In the weak-coupling limit for $\varepsilon_P \ll \varepsilon_c$ the value of y_0 is very small. Iterating Eq. (56) one can then write $y_0 \approx \frac{\varepsilon_P}{\varepsilon_c} \arctan[\frac{\varepsilon_P}{\varepsilon_c} \arctan(-\tilde{\varepsilon}_0) - \tilde{\varepsilon}_0]$ which has the correct small and

large $\tilde{\varepsilon}_0$ behavior. Keeping only the leading order one finds for the softening a Lorentzian behavior

$$\frac{\omega_m^2}{\omega_0^2} = 1 - \frac{(\varepsilon_P/\varepsilon_c)}{1 + \tilde{\varepsilon}_0^2}, \qquad (57)$$

as observed in experiments [27,28,36,37].

(ii) At criticality for $\varepsilon_P = \varepsilon_c$ Eq. (56) can be solved for $\tilde{\varepsilon}_0 \ll 1$ by expanding the right-hand side to third order. This gives $y_0 = \tilde{\varepsilon}_0 - (3\tilde{\varepsilon}_0)^{1/3}$ and consequently $\omega_m = \omega_0(3|\tilde{\varepsilon}_0|)^{1/3}$ that is singular at the transition.

Finally (iii) for $\varepsilon_P > \varepsilon_c$ and $\tilde{\varepsilon}_0 = 0$ there exist two (stable) solutions of Eq. (56) $y_0(\tilde{\varepsilon}_0 = 0) = \pm z_0$, with $z_0 > 0$. For small value of $\tilde{\varepsilon}_0 > 0$ one can find the solution of Eq. (56) as

$$y_0 = -z_0 + \frac{(\tilde{\varepsilon}_0/4)}{\varepsilon_P/\varepsilon_c - 1} \qquad (58)$$

that is valid for $0 < \tilde{\varepsilon}_0 \ll (\varepsilon_P/\varepsilon_c - 1)^{3/2}$. For $\tilde{\varepsilon}_0 < 0$ the stable solution is $-y_0$ [$y_0(\tilde{\varepsilon}_0) = -y_0(-\tilde{\varepsilon}_0)$], and sweeping $\tilde{\varepsilon}_0$ through 0 the system jumps from one solution to the other. We can thus simply concentrate on the positive values of $\tilde{\varepsilon}_0$. The linear dependence of y_0 leads to a linear dependence of ω_m^2 close to $\tilde{\varepsilon}_0 > 0$. For $0 < \varepsilon_P - \varepsilon_c \ll \varepsilon_c$ one finds

$$\frac{\omega_m}{\omega_0} = [2(\varepsilon_P/\varepsilon_c - 1)]^{1/2} + \frac{\tilde{\varepsilon}_0 \varepsilon_P}{2(\varepsilon_P - \varepsilon_c)}\left(\frac{3\varepsilon_c}{2\varepsilon_P}\right)^{1/2}. \qquad (59)$$

The slope diverges at $\varepsilon_P \to \varepsilon_c$, in agreement with the results at criticality that gives $\omega_m \tilde{\varepsilon}_0^{1/3}$. Since the curve is symmetric, the linear dependence leads to a cusp in the softening dependence on the gate voltage. This can be an indication of the bistability.

The results for $\varepsilon_P < \varepsilon_c$ and $\varepsilon_P > \varepsilon_c$ are shown in Figs. 5 and 6. The behavior discussed by simple analytical argument agrees with what is found by solving numerically Eq. (56) and substituting the result into Eq. (55) (dotted lines in both figures). As explained before, the calculation of the resonating frequency by this method gives only an indication of the mechanical dynamics, that is actually more complex. In the next subsection we thus discuss the form of the displacement and current spectrum taking into account the effect of the fluctuations.

B. Displacement spectra and current spectra as a function of $\tilde{\varepsilon}_0$

Using the numerical methods described above we obtain the displacement and current spectrum. For $\varepsilon_P \leqslant \varepsilon_c$ the displacement spectrum shows a clear peak at frequencies that are very close to the results obtained by the analytical method. The position of the peak is shown by the continuous lines in Fig. 5. For weak coupling the agreement is essentially perfect. For $\varepsilon_P = \varepsilon_c$ one sees instead that the peak remains at a higher energy. As we found for the case $\tilde{\varepsilon}_0 = 0$ in Ref. [38] the strong nonlinear form (x^4) of the potential at that point is at the origin of this difference. There the spectrum has a form

$$S_{xx}(\omega) = S_{xx}(\omega_M)\left(\frac{\omega}{\omega_M}\right)^4 e^{-[(\omega/\omega_M)^4-1]}, \qquad (60)$$

with $\omega_M \approx 1.212\omega_0(T_{\text{eff}}/\Gamma)^{1/4}$. The width of the peak is due to the phase fluctuation, and it is so wide since $\omega(E)$ given by Eq. (24) vanishes for $E = 0$.
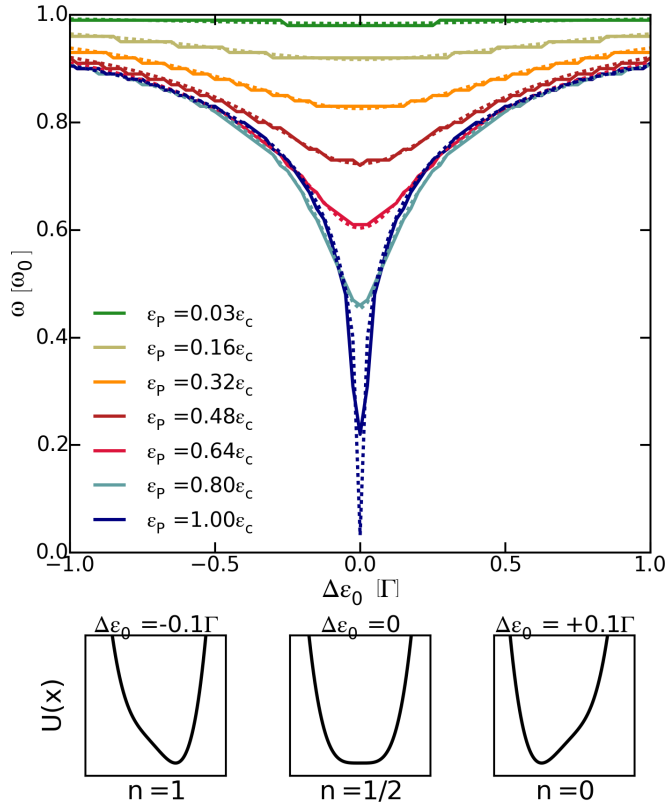
FIG. 5. Gate voltage dependence ($\tilde{\varepsilon}_0$) of the mechanical resonating frequency for different values of the coupling $\varepsilon_P \leqslant \varepsilon_c$, as indicated in the legend. The dotted lines indicate the numerical solution of the mean field Eqs. (56) and (55). The continuous lines indicate the positions of the maxima in the $S_{xx}(\omega)$ spectrum. The parameters are $\Gamma/\omega_0 = 10^3$, $V/\Gamma = 5 \times 10^{-3}$, $T = 0$. Lower panel: Sketch of the effective potential as a function of the oscillator's position for various values of the dot's detuning; n represents the occupation of the dot, and the vertical axis has a range of $4T_{\text{eff}}$.
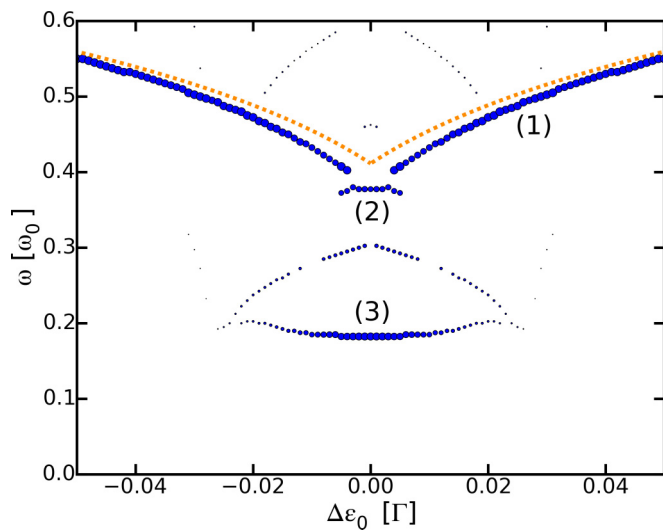

FIG. 6. Same as Fig. 5 but for $\varepsilon_P = 1.1\varepsilon_c$, corresponding to the bistable region. The orange dotted lines indicate the numerical solution of the mean field Eqs. (56) and (55). The dots indicate the positions of the dominant maxima in the $S_{xx}(\omega)$ spectrum, with a dot size proportional to the peak height.

At finite value of $\tilde{\varepsilon}_0$, the effective potential of the oscillator gets an asymmetric minimum (see lower panel of Fig. 5) which is responsible for a nonvanishing $\omega(E)$ at $E = 0$, as given by Eq. (55). This reduces the range over which the frequency can vary. As a consequence, at sufficiently large detuning $\tilde{\varepsilon}_0 \geqslant 0.1\Gamma$, the peak quite rapidly follows again the mean-field prediction shown by the light-blue dashed curve in Fig. 7 (left panel). For smaller dot-level detuning $\tilde{\varepsilon}_0 < 0.05\Gamma$, the spectrum becomes more complex, with the emergence of a secondary peak that is not described by the mean-field mode softening. This is due to the existence of a precise value of the energy $E_0 > 0$ (dependent on $\tilde{\varepsilon}_0$) for which the dispersion relation $\omega(E)$ of the oscillator develops a minimum. For $\omega \approx \omega(E_0)$ there is a square-root divergence of the spectrum $S_{xx}(\omega) \propto E_0 \sqrt{\omega''(E_0)/2[\omega - \omega(E_0)]}$. This divergence is further widened by dissipation and leads to a narrow peak, as shown by the dark-blue dashed curve in Fig. 7 (left panel). The double-peak feature rapidly disappears close to criticality, where one recovers the spectrum described by Eq. (60).

Particularly interesting is the case $\varepsilon_P > \varepsilon_c$. As we have seen analytically in Eq. (59), we expect a cusp in the mean-field peak position close to $\tilde{\varepsilon}_0 = 0$. This is also found numerically, as it can be seen from Fig. 6, branch (1), at least for $\tilde{\varepsilon}_0$ not too small. When we look more in detail close to $\tilde{\varepsilon}_0 = 0$, we find two minima in the effective potential, one stable and one metastable. We assign the peaks in branch (1) to oscillations around the stable minimum. The contribution of the metastable state rapidly vanishes due to its population, exponentially small in the regime $T_{\text{eff}} \ll \Gamma$. It can still be seen close to its merging with the stable-minimum peak, arising at branch (2). However, its presence is fundamental to generate branch (3), that is associated to oscillations around both minima and of which frequency is roughly half the frequency of branch (1).

We can calculate also the current spectrum. We show in Fig. 7 the result for $\varepsilon_P = \varepsilon_c$. In order to understand the relation with the displacement spectrum one can generalize Eq. (39):

$$
\begin{aligned}
\frac{S_{II}(t)}{(F_0/\Gamma)^2} \approx (G_Q V)^2 \tau^3 \bigg\{ & 4(1-\tau) S_{xx}(t) \\
& + \frac{\Gamma^2}{F_0^2} \tau (3 - 4\tau)^2 [\langle y^2(t) y^2(0) \rangle - \langle y^4(0) \rangle] \\
& + \frac{\Gamma^2}{F_0^2} 16(1-\tau)(1-2\tau) [\langle y(t) y^3(0) \rangle - \langle y^4(0) \rangle] \bigg\}.
\end{aligned}
$$
(61)

The first term in Eq. (61) is proportional to the mechanical noise $S_{xx}(t)$. It dominates the spectral signal for the detuned dot-level position ($\Delta\varepsilon_0 \neq 0$ and $\tau \neq 1$) and is at the origin of the double V shape seen in Fig. 7(b). The second and third terms in Eq. (61) are related to the fourth-order correlation functions of the oscillator position. The second term dominates the spectrum in the region close to the critical point ($\Delta\varepsilon_0 = 0$ and $\tau = 1$). The line shape in this regime is well reproduced by Eq. (49) giving the regular part of the spectral density. Finally, we remark on the presence of a low-frequency noise due to the singular part of the spectral density written in Eq. (50).
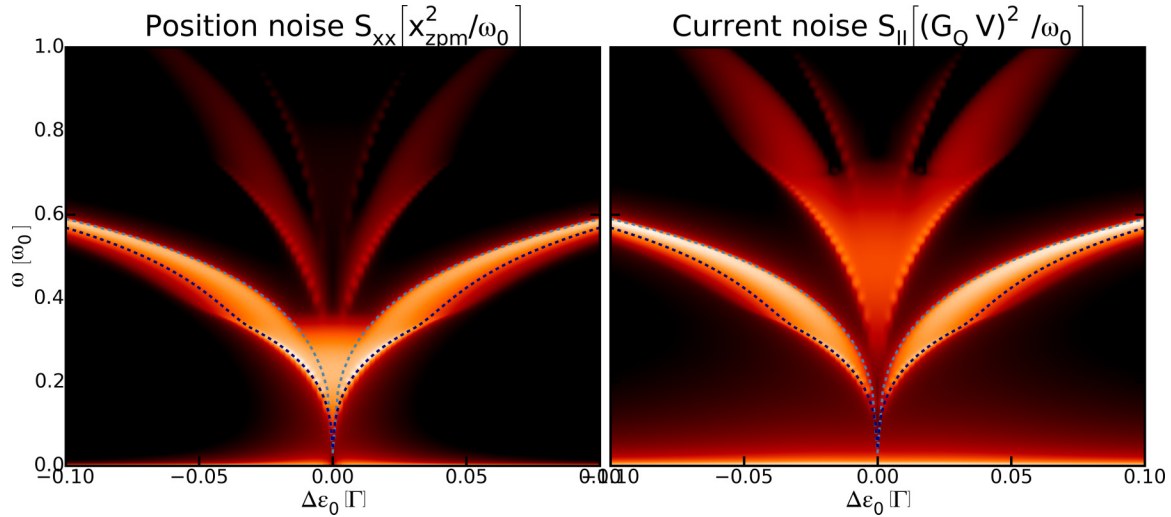
FIG. 7. Density plot of the displacement spectrum S_{xx} (left panel) and current spectrum S_{II} (right panel) as a function of dot-level detuning $\Delta\varepsilon_0$ and frequency ω. The dashed light-blue line shows the position of ω_m from the solution of Eqs. (56) and (55). The dashed dark-blue line shows the position of $\omega(E_0)$ at which the dispersion relation has a minimum. The maximum value in the density scale has been chosen according to the most important finite-frequency peak, and the minimum value has been chosen four orders of magnitude below. The plot is presented in logarithmic scale. Note that a zero-frequency noise peak is present and is typically several orders of magnitude above the max of the scale, especially in the current plot. The parameters are the same of the previous two figures.

To conclude, we have seen that the transition to the bistable phase can be detected by studying the displacement or current spectrum as a function of the detuning of the single-electron level. Specifically the shape of the softening depends strongly on the value of the interaction. A cusp should appear for coupling larger than the critical value. Clearly, fluctuations smoothen the transition, but the characteristic dependence on the bias voltage of the structures should be also a valuable indication of the true nature of the transition.

VI. TRANSITION AT FINITE TEMPERATURE

In this section we discuss the behavior of the system when the electronic leads are kept at finite temperature. Two different manifestations of the finite temperature are as follows: (i) The distribution of the electronic population of the metallic leads modifies the transport properties of the quantum dot and in particular its average electronic occupation $[\langle n(x)\rangle]$ that is responsible for the effective force acting on the oscillator. (ii) Thermal electronic fluctuations induce equilibrium fluctuations of $n(x)$ thus leading to a stochastic force that heats the oscillator even for $V = 0$.

A. Temperature dependence of the effective potential

Equation (3) gives the expression of the average electronic occupation of the dot. At finite temperature it can be expressed in terms of the digamma function (Ψ):

$$n = \frac{1}{2} + \frac{1}{2\pi}\text{Im} \sum_{\alpha=L,R} \Psi\left(\frac{1}{2} + \frac{\Gamma + i(\mu_\alpha - \epsilon_0 + F_0 x)}{2\pi T}\right). \tag{62}$$

We are interested in studying how the transition is modified by the temperature. For this we begin by considering the behavior of ω_m^2 as defined by Eq. (14). The change of sign of ω_m^2 indicates that the stationary point is no more stable. For

simplicity we focus on the $V = 0$ case. The critical value of the coupling constant for which $\omega_m^2 = 0$ reads then

$$\varepsilon_c(T) = -\left(\frac{\partial n}{\partial \epsilon_0}\right)^{-1} = \frac{2\pi^2 T}{\Psi^{(1)}(1/2 + \Gamma/2\pi T)}, \tag{63}$$

with $\Psi^{(n)}(z) = d^n\Psi(z)/dz^n$ the nth derivative of the digamma function and we consider only the case $\epsilon_0 = \varepsilon_P/2$. Using known properties of the digamma function $[\Psi^{(1)}(1/2) = \pi^2/2,$ $\Psi(z) \approx 1/z + 1/(2z^2) + 1/(6z^3) + \cdots$ for large $z]$, [46] one finds the asymptotic $T \gg \Gamma$ behavior,

$$\varepsilon_c(T \gg \Gamma) = \frac{4T}{1 + \Psi^{(2)}(1/2)\Gamma/(T\pi^3)}, \tag{64}$$

and the low-temperature one,

$$\varepsilon_c(T \ll \Gamma) = \pi\Gamma\left(1 + \frac{\pi^2}{3}\frac{T^2}{\Gamma^2}\right) \tag{65}$$

(the last expression can also be obtained by Sommerfeld expansion). One thus finds that the transition in principle can be also observed at high temperatures, provided a coupling constant of the order of $4T$. By a comparison with the result (11) for the bias voltage dependence of ε_c, one sees that the temperature (for $T \gg \Gamma$) is less effective in the renormalization of the spring constant. Clearly the same expressions allow one to study the evolution of ω_m:

$$\frac{\omega_m^2}{\omega_0^2} = 1 - \frac{\varepsilon_P}{\varepsilon_c(T)}. \tag{66}$$

At mean-field level the temperature simply changes the critical value of the coupling. The critical line (63) is shown in Fig. 8 (lower panel, full line). The dotted (orange) curve shows the low-temperature approximation (65).

To conclude the discussion we remark that not only the coefficient of the quadratic term in the effective potential
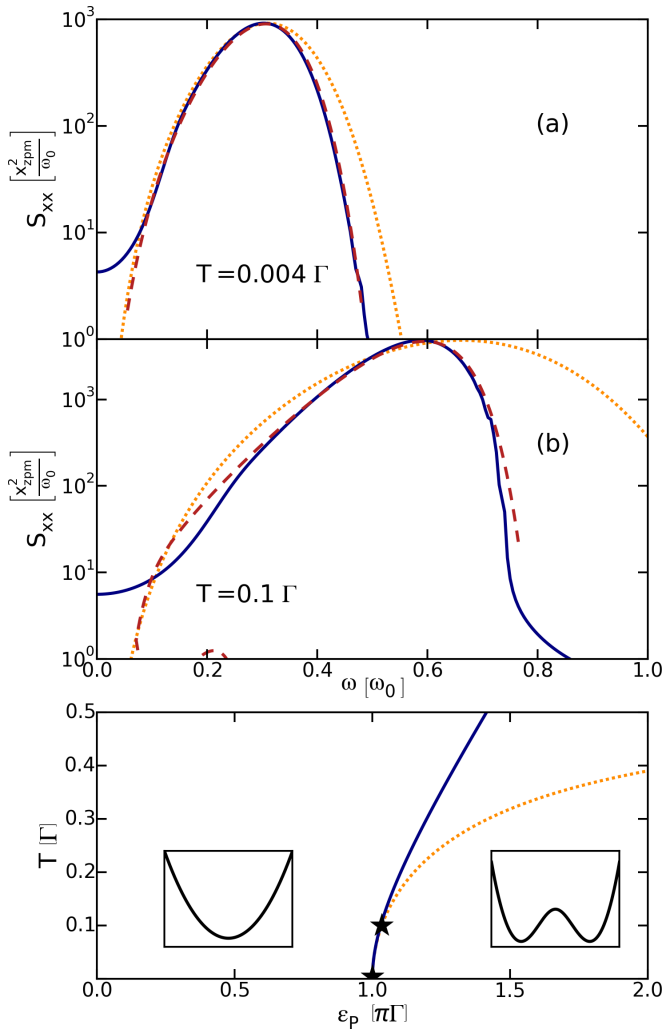
FIG. 8. Top panels: displacement spectrum $S_{xx}(\omega)$ for (a) $T/\Gamma = 4 \times 10^{-3}$ and (b) $T/\Gamma = 0.1$. Solid (blue) lines indicate the numerical results from Eq. (37), while dotted (orange) lines stand for the analytical low-temperature approximation of Eq. (60) with renormalized parameters. The dashed (red) lines correspond to evaluating numerically Eq. (40) for the mechanical noise, using the exact expression for the effective potential. Bottom panel: Phase diagram of the system in the plane T-ε_P. The bistability is present only in the area to the right of the transition, as is illustrated by the potential energy (see the insets). The analytical transition line for $T \ll \Gamma$ is shown in dotted (orange) line following Eq. (65). The two stars indicate the values at which the top panels are calculated. The parameters are the same of previous figures.

is modified by the temperature, but also the higher-order ones. Using the fact that $\Psi(z) = \ln \Gamma(z)/dz$ we can write an analytical expression also for the effective potential:

$$U(y) = \frac{\Gamma^2}{2\varepsilon_P} y^2 + 2T \operatorname{Re} \ln \Gamma \left[\frac{1}{2} + \frac{\Gamma}{2\pi T}(1 + iy) \right], \quad (67)$$

where we have used the dimensionless position y introduced above. One can verify using the asymptotic behavior for large z of $\ln \Gamma = z \ln z - z - \ln(z/2\pi)/2 + \cdots$ [46] that Eq. (67) reduces to Eq. (12) for $T \ll \Gamma$. The generic n term of the

expansion of $U(y) = \sum_{n=2}^{\infty} U_n y^n$ reads

$$U_n = \delta_{n,2} \frac{\Gamma^2}{2\varepsilon_P} + \frac{\Gamma}{\pi n!} \Psi^{(n-1)} \left(\frac{1}{2} + \frac{\Gamma}{2\pi T} \right) \left(\frac{\Gamma}{2\pi T} \right)^{n-1}, \quad (68)$$

with U_n nonvanishing only for n even. This gives immediately that the quartic term U_4 is always positive and vanishes for large T as $1/T^4$. In general the effective potential induced by the electrons vanishes for large temperature, since in this limit the average occupation of the dot, n, depends very weakly on the position of the level. In the opposite limit, for $T \ll \Gamma$, one finds for the quartic term of the expansion of $U(y)$: $U_4 = (\Gamma/12\pi)[1 - 2\pi^2(T/\Gamma)^2]$.

B. Effect of thermal fluctuations on mechanical noise

In thermal equilibrium ($V = 0$) the distribution function is always given by Eq. (18) with $T_{\text{eff}} = T$. One can thus obtain the spectrum of both I and x from expressions like Eq. (40). The only difference with the previous case is the form of the effective potential U that leads to a different expression for $\omega(E)$ and $x_E(t)$.

Specifically at the critical line the quadratic term vanishes and as far as the quartic term dominates over the higher-order terms the universal line shape for $S_{xx}(\omega)$ given in Eq. (60) holds. The only difference is the value of the maximum of the peak ω_M,

$$\omega_M(T) \approx 1.212 \omega_0 \left(\frac{T}{\Gamma} \right)^{1/4} \left[1 - \frac{\pi^2}{2} \left(\frac{T}{\Gamma} \right)^2 \right]. \quad (69)$$

Hence with increasing temperature, the maximum of the spectral line $S_{xx}(\omega)$ moves toward higher frequencies while its width increases.

In Fig. 8, upper panels, we plot the displacement spectrum $S_{xx}(\omega)$ obtained at two different temperatures $T/\Gamma = 4 \times 10^{-4}$ [panel (a)] and $T/\Gamma = 0.1$ [panel (b)]: The (orange) dotted line presents the analytical results given by Eq. (60) and the (blue) solid line presents the full numeric calculations given by Eq. (37). We observe that the analytical results are qualitatively consistent with the numerics: Namely, we find a shift of the peak toward higher frequencies and an enlarged broadening of the resonance upon increasing temperature. However a quantitative discrepancy is evident, especially at higher temperature [panel (b)]. This is due to the fact that by increasing the temperature the fluctuations increase and at some point the sixth- and higher-order terms cannot be neglected anymore. Let us assume that the distribution function is $P \sim e^{-U_4 y^4/T}$. We can then evaluate the contribution of any term in the expansion of $U(y)$:

$$\langle x^n \rangle = \frac{\Gamma[1/4 + n/4]}{\Gamma[1/4]} \left(\frac{T}{U_4} \right)^{n/4}. \quad (70)$$

We thus find that $U_n \langle x^n \rangle / (U_4 \langle x^4 \rangle) \sim (U_n/U_4)(T/U_4)^{(n-4)/4}$. From expression (68) one finds that for $T \to 0$ the coefficients $U_n \sim \Gamma$. This gives the condition $(T/\Gamma)^{(n-4)/4} \ll 1$ in order to neglect the term of order n with respect to the term of order 4. For the case in panel (b) the condition for the sixth terms reads $\sim \sqrt{T/\Gamma} \approx 0.3$. We verified that by evaluating numerically the expression equivalent to Eq. (40) for S_{xx} taking into account

the exact form of the potential (see dashed lines in the figure) we recover the results of the full numerical solution.

VII. EFFECTS OF A DISSIPATIVE COUPLING

Up to this moment, we considered the coupling with the electrons to be the only source of dissipation of the system. In this section we consider the effect of a coupling to a bath at the same temperature of the electronic degrees of freedom, but with an independent coupling constant modeled by the damping rate γ_e. The fluctuations induced by this coupling satisfy the fluctuation-dissipation theorem, leading to a modification of the Fokker-Planck Eq. (6) as follows:

$$\frac{A}{m} \to \frac{A}{m} + \gamma_e, \quad D \to D + 2\gamma_e mT. \quad (71)$$

In the limit $T, V \ll \Gamma$ the stationary solution is still of the Gibbs form (18) with effective temperature:

$$T_{\text{eff}}(\gamma_e) = \frac{D + 2m\gamma_e T}{2A + 2m\gamma_e} = \frac{T_{\text{eff}}(0) + Tm\gamma_e/A}{1 + m\gamma_e/A}. \quad (72)$$

From this expression one can conclude that for $m\gamma_e/A \ll 1$ and $Tm\gamma_e/A \ll T_{\text{eff}}(0)$ the effect of an additional dissipative channel can be neglected. Since $T_{\text{eff}}(0) \geqslant T$ as given by Eq. (20), the first condition is sufficient to neglect the effect of fluctuations.

When $m\gamma_e/A$ is not small there are two possibilities. If $T \gg V$, then one simply finds $T_{\text{eff}}(\gamma_e) = T_{\text{eff}}(0) = T$, independently of γ_e. More interesting is the opposite limit, of $T \ll V$, in this case $T_{\text{eff}}(0) = V/4$ and we find

$$T_{\text{eff}}(\gamma_e) = \frac{T_{\text{eff}}(0)}{1 + m\gamma_e/A}. \quad (73)$$

The effect of the dissipation is then to cool down the oscillator. This is not surprising: the presence of a voltage bias induces heating and by coupling the mechanical oscillator to the cold environment one can reduce the effective temperature. Thus we find that for the observation of the transition the presence of an additional (and in general unavoidable) dissipation is either uninfluential or an advantage (in the case $T \ll V$).

In order to see this we solve numerically the problem and show in Fig. 9 as a function of γ_e for $T = 0$ the dependence of the main peak position of $S_{xx}(\omega)$, its width, its quality factor Q, and the effective temperature of the system T_{eff}. One clearly sees that increasing the dissipation reduces the position of the main peak and its width, but the ratio remains perfectly constant, as shown by the evolution of the quality factor. All the dependence can be explained by the renormalization of the effective temperature predicted by Eq. (73).

The only point that requires some additional explanation is the way the peak becomes overdamped when $\gamma_e \approx \omega_M$. We found that this can be understood in terms of a simple model. Let us consider the displacement spectrum for a damped harmonic oscillator of frequency ω_t and damping γ driven by a force noise $\xi(t)$: $S_{xx}(\omega) = [|\xi(\omega)|^2/m^2][(\omega^2 - \omega_t^2)^2 + \omega^2\gamma^2]^{-1}$. Assuming a white noise $\xi(\omega) \approx \xi(0)$ we find that $S_{xx}(\omega)$ has two maxima at $\omega = \pm\omega_1$ with

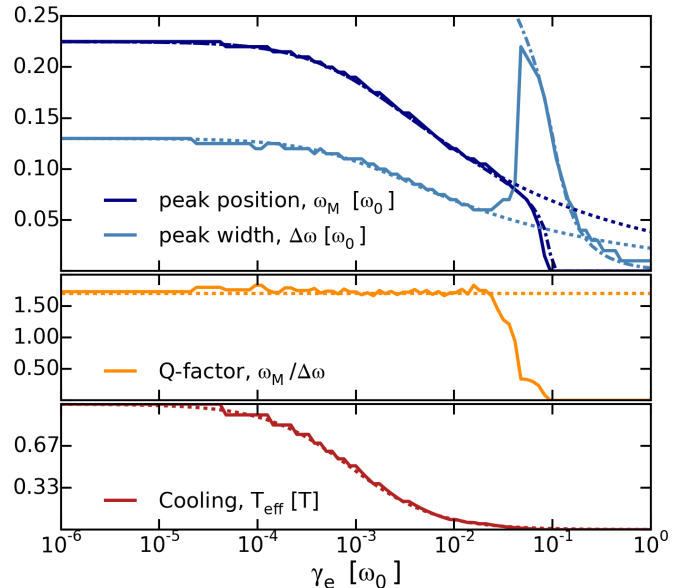$$\omega_1 = (\omega_t^2 - \gamma^2/2)^{1/2} \quad (74)$$

FIG. 9. We plot as a function of the damping constant γ_e the position and the width of the maximum of $S_{xx}(\omega)$ (upper panel), the quality factor (middle panel), and the effective temperature T_{eff} (lower panel). Solid lines represent the numerical results obtained by solving the Fokker-Planck equation. The dashed lines in the upper and central panels indicate the evolution of ω_m and $\Delta\omega$ given by the analytical expression $\omega_M = 1.2\omega_0(T_{\text{eff}}/\Gamma)^{1/4}$ and $Q = \omega_M/\Delta\omega = 1.71$ valid at criticality. The dot-dashed line in the upper panel is given by Eqs. (75) and (74). The parameters are $\Gamma = 1000\omega_0$, $\varepsilon_P = \varepsilon_c$, $T = 0$, and $V/\Gamma = 5 \times 10^{-3}$.

for $\gamma < \sqrt{2}\omega_t$ and a single maximum at $\omega = 0$ for $\gamma \geqslant \sqrt{2}\omega_t$. Assuming that ω_M plays the role of ω_t we plot as a dot-dashed line in the upper panel of Fig. 9 the expected behavior of the maximum on $S_{xx}(\omega)$ as predicted by Eq. (74). This agrees remarkably well with the full numerics, even if the origin of the peak is due to quartic fluctuations. We think that the reason is that the dissipation dominates, thus it is not very important the origin of the peak. Pushing even further the model in the overdamped regime we looked at the evolution of the peak by calculating the value of ω for which $S_{xx}(\omega_2) = S_{xx}(0)/2$. We find

$$\omega_2 = \left[\omega_t^2 - \frac{\gamma^2}{2} + \sqrt{\left(\omega_t^2 - \frac{\gamma^2}{2}\right)^2 + \omega_t^4} \right]^{1/2}. \quad (75)$$

We compare then $2\omega_2$ with the full width half maximum found numerically. Note that numerically when the peak has only one side that allows us to find the half value we simply double the distance from the maximum to this frequency. Again a comparison of the linear model and the full numerics works remarkably well.

VIII. CONCLUSIONS

In this paper we have studied the transition to a mechanical bistability induced by the strong coupling between a mechanical degree of freedom and the charge in a quantum dot. We have considered the experimentally relevant regime of $\Gamma \gg \omega_0$. We have studied the phase diagram of the problem as a function

of the bias voltage (cf. Fig. 1), the temperature (cf. Fig. 8), and the gate voltage (cf. Figs. 5 and 6). The critical value of the coupling ε_c to observe the transition depends on the voltage quadratically [cf. Eq. (11)] and on the temperature linearly [cf. Eq. (63)]. Since reaching large coupling is a difficult experimental problem, the ideal situation for the observation of the transition is the low-temperature and low bias voltage case for which $\varepsilon_c = \pi \Gamma$. We investigated this limit in a previous publication [38]. One of the main messages was that the mechanical degrees of freedom had a much stronger response at the transition than the electronic ones. To clarify better this point in the present paper we considered in detail the behavior of the conductance (cf. Fig. 3). We find that it has a singular behavior at exactly vanishing temperature and bias voltage, but in practice it becomes smooth very rapidly when $V > 0$ and it has a slow power-law decrease for large coupling. Thus for sufficiently large coupling this leads to a well defined blockade [19], but in the range relevant for the present experiments the conductance does not provide an unambiguous proof of the bistability. For this reason we investigate in detail the quantities that are directly related to the mechanical degrees of freedom. The main effect at the transition is the softening of the mechanical mode as predicted by the behavior of the electronic effective potential. This is reflected in the response function to an external driving force, in the ring-down time, and in particular in the displacement fluctuation spectrum $S_{xx}(\omega)$ [38]. Here we have investigated in detail the behavior of the current-spectral density $S_{II}(\omega)$. This quantity has been measured for suspended carbon nanotubes [33]. We found that measurement of $S_{II}(\omega)$ can give a direct access to $S_{xx}(\omega)$, but in a simple way only deep in the bistable phase. Actually in the most interesting case of resonant tunneling ($\Delta\epsilon_0 = 0$) the transparency of the junction depends quadratically on the displacement, leading to a relation (44) between S_{II} and S_{xx}, that breaks down at the transition due to the strong nonlinearity. One can nevertheless obtain the behavior of the current noise, that has similar remarkable features of S_{xx} at the transition [cf. Eqs. (49) and (50)]. The behavior of the peak position (ω_M) and of its width constitutes robust fingerprints of the transition.

We investigated the role of a detuning of the dot level $\Delta\varepsilon_0$ and of a finite temperature T on this critical behavior. We showed that the dependence of the mode softening with $\Delta\varepsilon_0$ is extremely sharp close to criticality, scaling with $(3|\Delta\epsilon_0|/\Gamma)^{1/3}$. This is in striking contrast with the Lorentzian behavior expected in the weak-coupling limit and actually observed in all current experiments. We found that the main effect of the temperature is to change the value of the critical coupling needed to observe the transition and, of course, to increase the fluctuations by changing the effective temperature. Finally we showed that the effect of a dissipation not due to the electrons is actually in general useful to keep the oscillator cold in the case where the voltage bias is larger than the electronic temperature.

We gave thus a global picture of the transition, investigating the main physical quantities, and showing that several features can be used to characterize without ambiguity the transition to the bistable state. These results give clear indications opening the way to the observation of this phenomenon with state-of-the-art experiments.

The experimental observation of the transition would indicate that one has entered a completely different regime, where the interaction due to a single electron has a dramatic effect on transport and mechanical behavior. In molecular devices these kinds of effects might have been observed [47–50], but in these systems is nearly impossible to tune the electron-phonon coupling. Observation of the transition in nanoelectro mechanical systems, like the suspended carbon nanotubes, would then open the way to controlled investigations of the strong-coupling regime. The increase in the coupling leads naturally to an increase in the sensitivity of the detection, with improvement in the sensitivity of the device (for instance for mass or force detection). From the fundamental point of view, a better understanding of the behavior of mechanical resonators in the ultrastrong coupling regime could pave the way for testing decoherence [51] as well as reaching the ultimate limits in the control of mechanical motion at the nanoscale [52].

From the theoretical point of view there are still open questions. At the moment it is difficult to perform experiments in the quantum regime ($\omega_0 \sim T$), but the observation of very high-frequency mechanical resonators [32] leaves open the possibility of reaching at some point this limit and thus should motivate theoretical studies. An even more stringent question is opened by a recent publication [53], where by mapping the quantum problem to an effective Kondo problem it was shown that the bistability in the quantum regime may be washed out. The study was performed in equilibrium and focused only on the probability distribution. An investigation of the response functions S_{xx} in that regime would be extremely interesting in order to clarify the expected evolution of measurable quantities at the transition for low temperatures.

ACKNOWLEDGMENT

APPENDIX: DERIVATION OF ⟨n⟩ AND ⟨n(t)n(0)⟩

In this Appendix we present a derivation [54] of the $\langle n \rangle$ and $\langle n(t)n(0) \rangle$ based on the method known as input-output theory widely used in quantum optics for bosonic fields (see for instance Ref. [55]), but much less used to describe fermions. We consider the Hamiltonian (1) for given $\epsilon_d = \epsilon_0 - F_0 x$: x here is a constant c number. The Hamiltonian is quadratic in the fermionic operators. One can then calculate exactly all correlation functions. We begin by writing the equation of motions for the fermionic operators in the Heisenberg representation:

$$\dot{d}(t) = -i\epsilon_d \, d(t) - i \sum_{\alpha k} t_\alpha^* \, c_{\alpha k}(t)$$

$$\dot{c}_{\alpha k}(t) = -i\epsilon_{\alpha k} \, c_{\alpha k}(t) - i t_\alpha \, d(t). \tag{A1}$$

It is convenient to introduce new operators: $\tilde{d}(t) = \exp(i\epsilon_d t)d(t)$ and $\tilde{c}_{\alpha k}(t) = \exp(i\epsilon_d t)c_{\alpha k}(t)$. In terms of these operators we can solve the second of the two equations (A1):

$$\tilde{c}_{\alpha k}(t) = -i t_\alpha \int_0^t e^{-i\Delta_{\alpha k}(t-t')}\tilde{d}(t')dt' + e^{-i\Delta_{\alpha k}t}\tilde{c}_{\alpha k}(0), \tag{A2}$$

where we have defined the energy difference $\Delta_{\alpha k} = \epsilon_{\alpha k} - \epsilon_d$ and $\tilde{c}_{\alpha k}(0)$ is the initial condition for the equation. Substituting the form (A2) into Eq. (A1) we have

$$\dot{\tilde{d}}(t) = -\sum_{\alpha k} \left[|t_\alpha|^2 \int_0^t e^{-i\Delta_{\alpha k}(t-t')} \tilde{d}(t') dt' + it_\alpha^* e^{-i\Delta_{\alpha k}t} \tilde{c}_{\alpha k}(0) \right].$$
(A3)

Since the leads are metallic the summation over k can be replaced by an integration over the energy by defining the density of states of the system: $\rho_\alpha(\nu_\alpha) = \sum_k \delta(\nu_\alpha - \Delta_{\alpha k})$. In the wide-band approximation we neglect the energy dependence of the density of states and we obtain

$$\sum_k |t_\alpha|^2 \int_0^t dt' e^{-i\Delta_{\alpha k}(t-t')} = 2\Gamma_\alpha \, \delta(t-t'),$$

where we have introduced Γ_α as defined in Sec. II.

It is convenient to define an incoming field:

$$\tilde{c}_{\alpha,\text{in}}(t) = \sum_k e^{-i\Delta_{\alpha k}t} c_{\alpha k}(0).$$
(A4)

Defining $t_\alpha = |t_\alpha| \, \exp(-i\phi_\alpha)$ we have

$$\dot{\tilde{d}}(t) = -\Gamma \tilde{d}(t) - \sum_\alpha i e^{-i\phi_\alpha} (\Gamma_\alpha/\pi \, \rho_\alpha)^{1/2} \tilde{c}_{\alpha,\text{in}}(t)$$
(A5)

that can be solved by Fourier transform:

$$\tilde{d}(\omega) = -i\chi(\omega) \sum_\alpha e^{i\phi_\alpha} (\Gamma_\alpha/\pi \, \rho_\alpha)^{1/2} \, \tilde{c}_{\alpha,\text{in}}(\omega),$$
(A6)

where we have defined $\chi(\omega) = (i\omega + \Gamma)^{-1}$.

In order to be able to compute the correlation functions we need to specify the averages of the c operators for $t = 0$. We assume that the Fermions are in thermal equilibrium for $t = 0$:

$$\langle c_{\alpha,k}^\dagger(t) c_{\beta,k'}(0) \rangle = \delta_{\alpha,\beta} \delta_{k,k'} e^{i\epsilon_{\alpha k}t} f_F(\epsilon_{\alpha k} - \mu_\alpha), \quad \text{(A7)}$$

$$\langle c_{\alpha,k}(t) c_{\beta,k'}^\dagger(0) \rangle = \delta_{\alpha,\beta} \delta_{k,k'} e^{-i\epsilon_{\alpha k}t} [1 - f_F(\epsilon_{\alpha k} - \mu_\alpha)]$$
(A8)

with vanishing $\langle cc \rangle$ and $\langle c^\dagger c^\dagger \rangle$ and where we have defined the Fermi distribution function $f_F(\epsilon) = 1/(1 + e^{\epsilon/T})$. One can then obtain the form of the correlation function for d:

$$\langle d^\dagger(\tau) \, d(0) \rangle_\omega = 2|\chi(\omega - \epsilon_d)|^2 \sum_\alpha \Gamma_\alpha \, f_\alpha(\omega),$$
(A9)

where $f_\alpha(\omega) = f_F(\omega - \mu_\alpha)$.

At equal time ($t = 0$) Eq. (A9) gives the average charge on the dot,

$$\langle n \rangle = 2 \int_{-\infty}^{+\infty} \frac{d\omega}{2\pi} \frac{\Gamma_L f_L(\omega) + \Gamma_R f_R(\omega)}{\Gamma^2 + (\omega - \epsilon_d)^2},$$
(A10)

that leads to Eq. (3) in the main text.

We consider now $S_{nn}(t)$. By using Wick's theorem we can write it as a product of two correlation functions of the form (A9): $S_{nn}(t) = \langle d^\dagger(t)d(0)\rangle \langle d(t)d^\dagger(0)\rangle$. The Fourier transform gives then

$$S_{nn}(\omega) = \sum_{\alpha,\beta} \int_{-\infty}^{+\infty} \frac{d\omega'}{2\pi} \frac{2\Gamma_\alpha f_\alpha(\omega')}{\Gamma^2 + (\omega' - \epsilon_d)^2} \cdot$$

$$\times \frac{2\Gamma_\beta [1 - f_\beta(\omega' - \omega)]}{\Gamma^2 + (\omega' - \omega - \epsilon_d)^2}$$
(A11)

from which the expressions Eqs. (4) and (5) can be derived.

[1] M. Roukes, Scientific American **17**, 4 (2007).

[2] H. J. Mamin, M. Poggio, C. L. Degen, and D. Rugar, Nat. Nanotechnol. **2**, 301 (2007).

[3] B. Lassagne, D. Garcia-Sanchez, A. Aguasca, and A. Bachtold, Nano Lett. **8**, 3735 (2008).

[4] P. Rabl, S. J. Kolkowitz, F. H. L. Koppens, J. G. E. Harris, P. Zoller, and M. D. Lukin, Nat. Phys. **6**, 602 (2010).

[5] I. Mahboob, K. Nishiguchi, H. Okamoto, and H. Yamaguchi, Nat. Phys. **8**, 387 (2012).

[6] I. Mahboob, K. Nishiguchi, A. Fujiwara, and H. Yamaguchi, Phys. Rev. Lett. **110**, 127202 (2013).

[7] J. Moser, J. Güttinger, A. Eichler, M. J. Esplandiu, D. E. Liu, M. I. Dykman, and A. Bachtold, Nat. Nanotechnol. **8**, 493 (2013).

[8] M. Aspelmeyer, T. J. Kippenberg, and F. Marquardt, Rev. Mod. Phys. **86**, 1391 (2014).

[9] V. Sazonova, Y. Yaish, H. Üstünel, D. Roundy, T. A. Arias, and P. L. McEuen, Nature (London) **431**, 284 (2004).

[10] M. Galperin, M. A. Ratner, and A. Nitzan, Nano Lett. **5**, 125 (2005).

[11] D. Mozyrsky, M. B. Hastings, and I. Martin, Phys. Rev. B **73**, 035104 (2006).

[12] A. D. Armour, M. P. Blencowe, and Y. Zhang, Phys. Rev. B **69**, 125313 (2004).

[13] Y. M. Blanter, O. Usmani, and Y. V. Nazarov, Phys. Rev. Lett. **93**, 136802 (2004).

[14] N. M. Chtchelkatchev, W. Belzig, and C. Bruder, Phys. Rev. B **70**, 193305 (2004).

[15] A. A. Clerk and S. Bennett, New J. Phys. **7**, 238 (2005).

[16] C. B. Doiron, W. Belzig, and C. Bruder, Phys. Rev. B **74**, 205336 (2006).

[17] O. Usmani, Y. M. Blanter, and Y. V. Nazarov, Phys. Rev. B **75**, 195312 (2007).

[18] F. Pistolesi and S. Labarthe, Phys. Rev. B **76**, 165317 (2007).

[19] F. Pistolesi, Y. M. Blanter, and I. Martin, Phys. Rev. B **78**, 085127 (2008).

[20] G. Weick, F. Pistolesi, E. Mariani, and F. von Oppen, Phys. Rev. B **81**, 121409 (2010).

[21] G. Weick, F. von Oppen, and F. Pistolesi, Phys. Rev. B **83**, 035420 (2011).

[22] J. Brüggemann, G. Weick, F. Pistolesi, and F. von Oppen, Phys. Rev. B **85**, 125441 (2012).

[23] S. Braig and K. Flensberg, Phys. Rev. B **68**, 205324 (2003).

[24] J. Koch and F. von Oppen, Phys. Rev. Lett. **94**, 206804 (2005).

[25] J. Koch, F. von Oppen, and A. V. Andreev, Phys. Rev. B **74**, 205438 (2006).

[26] R. Leturcq, C. Stampfer, K. Inderbitzin, L. Durrer, C. Hierold, E. Mariani, M. G. Schultz, F. von Oppen, and K. Ensslin, Nat. Phys. **5**, 327 (2009).

[27] B. Lassagne, Y. Tarakanov, J. Kinaret, D. Garcia-Sanchez, and A. Bachtold, Science **325**, 1107 (2009).

[28] G. A. Steele, A. K. Hüttel, B. Witkamp, M. Poot, H. B. Meerwaldt, L. P. Kouwenhoven, and H. S. J. v. d. Zant, Science **325**, 1103 (2009).

[29] J. Chaste, A. Eichler, J. Moser, G. Ceballos, R. Rurali, and A. Bachtold, Nat. Nanotechnol. **7**, 301 (2012).

[30] M. Ganzhorn, S. Klyatskaya, M. Ruben, and W. Wernsdorfer, ACS Nano **7**, 6225 (2013).

[31] P. M. Kosaka, V. Pini, J. J. Ruz, R. A. d. Silva, M. U. González, D. Ramos, M. Calleja, and J. Tamayo, Nat. Nanotechnol. **9**, 1047 (2014).

[32] E. A. Laird, F. Pei, W. Tang, G. A. Steele, and L. P. Kouwenhoven, Nano Lett. **12**, 193 (2011).

[33] J. Moser, A. Eichler, J. Güttinger, M. I. Dykman, and A. Bachtold, Nat. Nanotechnol. **9**, 1007 (2014).

[34] A. Eichler, J. Moser, J. Chaste, M. Zdrojek, I. Wilson-Rae, and A. Bachtold, Nat. Nanotechnol. **6**, 339 (2011).

[35] Y. Zhang, J. Moser, J. Güttinger, A. Bachtold, and M. I. Dykman, Phys. Rev. Lett. **113**, 255502 (2014).

[36] J. Waissman, M. Honig, S. Pecker, A. Benyamini, A. Hamo, and S. Ilani, Nat. Nanotechnol. **8**, 569 (2013).

[37] A. Benyamini, A. Hamo, S. V. Kusminskiy, F. von Oppen, and S. Ilani, Nat. Phys. **10**, 151 (2014).

[38] G. Micchi, R. Avriller, and F. Pistolesi, Phys. Rev. Lett. **115**, 206802 (2015).

[39] F. Pistolesi, J. Low Temp. Phys. **154**, 199 (2009).

[40] R. Avriller and A. Levy Yeyati, Phys. Rev. B **80**, 041309 (2009).

[41] G. Piovano, F. Cavaliere, E. Paladino, and M. Sassetti, Phys. Rev. B **83**, 245311 (2011).

[42] Y. M. Blanter, O. Usmani, and Y. V. Nazarov, Phys. Rev. Lett. **94**, 049904(E) (2005).

[43] M. I. Dykman and M. A. Krivoglaz, Physica A: Stat. Mech. Appl. **104**, 480 (1980).

[44] M. Dykman and M. Krivoglaz, Physica A: Stat. Mech. Appl. **104**, 495 (1980).

[45] Y. M. Blanter and M. Büttiker, Phys. Rep. **336**, 1 (2000).

[46] *Handbook of Mathematical Functions: With Formulas, Graphs, and Mathematical Tables*, edited by M. Abramowitz and I. A. Stegun, 9th ed., Dover Books on Mathematics (Dover, New York, 2013).

[47] N. Tao, Nat. Nanotechnol. **1**, 173 (2006).

[48] E. Lörtscher, J. W. Ciszek, J. Tour, and H. Riel, Small **2**, 973 (2006).

[49] B.-Y. Choi, S.-J. Kahng, S. Kim, H. Kim, H. W. Kim, Y. J. Song, J. Ihm, and Y. Kuk, Phys. Rev. Lett. **96**, 156106 (2006).

[50] J. Gaudioso, L. J. Lauhon, and W. Ho, Phys. Rev. Lett. **85**, 1918 (2000).

[51] A. J. Leggett, J. Phys.: Condens. Matter **14**, R415 (2002).

[52] M. Poot and H. S. J. van der Zant, Phys. Rep. **511**, 273 (2012).

[53] J. Klatt, L. Mühlbacher, and A. Komnik, Phys. Rev. B **91**, 155306 (2015).

[54] F. Pistolesi, Lectures Presented at Casimir Research School, San Sebastiàn, Spain, 2014.

[55] D. F. Walls, G. J. Milburn, and Walls-Milburn, *Quantum Optics*, 2nd ed. (Springer, Berlin, 2008).